Model for avalanches in three spatial dimensions: comparison of theory to experiments

R. M. LANG
U.S. Army Cold Regions Research & Engineering Laboratory 72 Lyme Road, Hanover, N.H., 03755-1290, U.S.A.
Brian R. LEO
Sigma Technologies, Inc., 6970 Ford Dr. N.W., Gig Harbor, WA 98335, U.S.A.

INTRODUCTION

Increases in land use and development in mountainous areas, anticipated warming of the earth's atmosphere, and the deforestation in alpine regions from air pollution, acid rain, previously poor forestry practices, and land misuse have renewed attention to the importance of reliably recognizing natural avalanche paths and predicting deposition zones. The impact pressures induced by an avalanche in the runout area motivate zoning restrictions and building code requirements. Existing avalanche models are generally inadequate. Therefore, the current trend in the research of flowing snow and other materials is still directed at determining the predominant mechanisms governing the motion.

The phenomena collectively referred to as avalanches can be physically characterized as multiphase gravity flows, which consist of randomly dispersed, interacting phases, whose properties change with respect to both time and space. Lang and Dent (1982) describe an avalanche as "the transient, three-dimensional motion of a variable mass system made up of nonrigid, nonrotund, nonuniform assemblage of granular (snow) fragments flowing down a nonuniform slope of varying surface resistance." In this sense, an exact analysis of the motion of an avalanche is perhaps an unattainable goal.

Currently, the most widely used and applied avalanche models utilize a center of mass approach (i.e., the mass is accretized at one point) and are based on ideas first suggested by Voellmy (1955). By using the Prandtl mixing length approach (see for example Pao 1961), Voellmy related the stress at the base of the flow to the square of the velocity, and then postulated an additional Coulomb friction force. However, he assumed uniform, steady conditions and derived a method that is difficult to apply, in the sense that a number of subjective parameters must be predetermined in order to obtain results that match observational data. Although Voellmy's model has been successively improved (Salm 1966, Mellor 1968, Perla et al. 1980), these models have not advanced beyond the aforementioned center of mass approach. The height of the flow may be included as a parametric value, but is not calculated as a function of space and time.

Other models attempt to idealize these complicated materials as linear Newtonian fluids (Brugnot 1979, Dent and Lang 1980), leading to the Navier-Stokes equations that may be solved numerically. Although this type of constitutive relation perhaps should not be assumed to adequately describes these media, some success has been achieved in modeling certain aspects of avalanche behavior with this approach. Apparent viscosities may be measured for fluidized solids (e.g. Siemes and Hellmer, 1962). The ease with that particles fluidize and the range of conditions that sustain fluidization vary greatly among solid-fluid gravity current systems.

When considering snow avalanches in particular, due to the nonlinear behavior, and strong stress and strain history dependence of snow, constitutive equations tend to be quite complicated. Both continuum theories (Salm 1971, 1975, 1977, Brown et al. 1973, Brown and Lang 1973, Brown 1976, 1977, 1979, 1980a, 1980b) and microstructural theories (St. Lawrence 1977, St. Lawrence and Lang 1981, Hansen and Brown 1986, Hansen 1985) have

been proposed and applied successfully to various, specific problems in snow mechanics. But to some extent all require detailed information on the particular snow type in question, that entails a wide range of possible parametric values.

Another hindering factor has been the availability of experimental data on avalanche motion. Field measurements are limited and difficult to obtain (see, for example, Norem et al. 1985, Gubler 1987), and similitude is difficult to achieve when attempting to scale-down and model such flows in the laboratory. For example, Lang and Dent (1980) utilized a 1/100 scale model of snow, and successfully matched the Froude number, but not the Reynolds number. This is not an unusual problem in scale modelling when the same "fluid" is used. For a scale model with length $1/n$ of the prototype, equality of the Reynolds number requires a model characteristic speed of $v_m = n\, v_p$, where v_p is the prototype characteristic speed. Equality of the Froude number requires $v_m = v_p / \sqrt{n}$. Both requirements cannot be satisfied by using the same "fluid" in both model and prototype. Other recent attempts to scale model avalanche flow include Nakamura et al. (1987), Plüss (1987), Hutter et al. (1988), and Lang et al. (1989).

Savage and Hutter (1989) demonstrated that one may adequately describe a flowing mass of cohesionless, granular medium as an incompressible continuum that obeys a Mohr-Coulomb yield criterion. If the moving mass is assumed to be long and thin, a nondimensionalization scheme (resembling shallow-water theory) may be employed, which renders more tractable governing equations. By neglecting the boundary layer, a classical approximation method (first introduced by von Kármán (1921) and later refined by Pohlhausen (1921)) is employed, in that the equations are averaged over depth and a velocity profile is assumed. By defining a depth-averaged streamwise velocity and assuming incompressibility, these equations may be reliably solved with a Lagrangian finite difference scheme, such that the computational grid is advected with the material.

The purpose of this investigation was to extend this theory to three spatial dimensions and allow for the inclusion of a boundary drag term, and test its applicability against experimental results. The governing equations are derived in a curvilinear coordinate system that allows for topography to vary as in a natural avalanche path. The only assumptions included in the development are incompressibility and the application of a Mohr-Coulomb type material law, while also allowing the inclusion of a boundary drag term. A nondimensionalization scheme is employed, choosing three characteristic length scales. By depth and width averaging the balance equations for the theory in three spatial dimensions, sidewise spreading of the mass may be included. A Lagrangian finite difference scheme is applied to numerically integrate the sets of equations that are derived. The numerical simulations are then compared to the laboratory findings. The experimental results have been presented in Lang et al. (1989).

The analytical results indicate that a flow transition regime exists that is analogous to a laminar to turbulent transition in a fluid, and determines the applicability of the boundary drag term. Results are reviewed and suggestions are made for appropriate investigations implied by these results.

MATHEMATICAL FORMULATION

The governing equations and closure relations are proposed to represent the flow of a cohesionless granular medium on any given topography. By describing granular media as multiphase materials, intraphase balance equations for mass, momentum, and energy and the associated boundary and initial conditions may, in principle, be written. But the resulting set of equations is usually too complicated to allow for a solution. For example, the application of kinetic theories for granular flow would in general require the solution of the energy equation, determination of granular temperatures, and velocity and density gradients. Szidarovsky et

al. (1987) discuss the inherent difficulties in attempting to apply these theories to chute flows of granulate. Furthermore, such information is inappropriate for an engineering application.

The goal is therefore to develop a simple model to predict the flow characteristics of the mass of granulate. A purely mechanical theory is proposed and the granular mass is treated as a continuum. The concept of representing the granulate as a continuum should pose no conceptual problem, as a mixture theory approach would require the sum of the phase interaction terms to vanish in the overall balance equations, in any case.

The requisite is a suitable constitutive assumption. In order to justify the following approach, it is necessary to consider the different flow regimes in question, and also the experimental results from other investigations.

First, two extreme flow regimes for granular media are commonly recognized (see, for example, Savage 1984). At very low shear rates, a granulate may be characterized as a Mohr-Coulomb material. This implies quasistatic deformation, to some degree. The Mohr-Coulomb law is the basis of Critical State Soil Mechanics (CSSM), and is commonly referred to as the rupture condition; i.e., it implies impending plastic flow for a static soil mass, as it predicts the limit equilibrium when the shear stress is equal to the shear strength of the noncohesive soil. Simply stated, the maximum ratio of the shear to normal stress is equated to the tangent of the internal friction angle φ of the granulate. For slowly flowing masses of granulate, the bed shear stress results from the dry friction forces at the particle contacts, and the Coulomb failure criterion adequately describes these types of flows.

When shear rates are very high and particles are widely dispersed, instantaneous collisions dominate the behavior of the granulate. Interparticle and particle-bed contacts are brief, and the fluctuating part of the particle motion cannot be neglected. Kinetic theories predict quadratic dependence of stress on shear-rate, for rapidly shearing highly dispersed particulate, and this seems to provide good agreement with the available laboratory data. This extreme case may be used to describe the behavior of the dust cloud, which only serves to obscure the true nature of the avalanche, but does not represent any type of snow avalanche activity that could be construed as destructive, and need not be considered.

The real avalanche flow situation in most cases may develop from a low shear rate flow into an intermediate regime where both long-term particle contact and instantaneous interparticle collisions contribute to the generation of stresses. This was shown to be the case in the previously discussed experiments in Lang et al. (1989), for the artificial avalanches released at angles exceeding 35°. Observations (Dent and Lang 1981) and Doppler radar measurements (Gubler 1987) on natural snow avalanches confirm that a dense slowly deforming mass rides on a rapidly shearing layer, and may or may not be encompassed by a highly suspended dust cloud. This type of flow is more difficult to handle theoretically, as the exact mechanisms have not yet been clearly defined. Savage (1983) suggested representing the total stresses as a linear sum of the rate-independent dry friction and a rate-dependent "viscous" part. The question remains as to how the dynamic friction angle actually changes at lower volume fractions and higher shear rates. Following the work of Savage and Hutter (1989), the governing equations of mass and momentum balance are derived in three spatial dimensions in a coordinate system that allows for any given topography. An angle ζ is defined such that ζ is a function of x^1, the longitudinal direction, and defines the local inclination angle of the generatrix,

$$\zeta = \zeta\,(x^1) \quad . \tag{1}$$

It is then possible to define Cartesian components z^i in terms of the curvilinear coordinates x^i and the natural basis $\{\ \underline{g}_i\ \}$. An orthonormal basis $\{\ \underline{\hat{e}}_i\ \}$ in terms of the covariant components of the metric or fundamental tensor of the space $g_{m\,n} = \underline{g}_m \cdot \underline{g}_n$ is defined and applied.

The Eulerian form for mass balance is

$$\frac{d\,\rho(\underline{x},t)}{d\,t} + \rho(\underline{x},t)\ \vec{\nabla}_x \cdot \underline{v}\,(\underline{x},t) = 0 \quad . \tag{2}$$

In terms of the physical components of $\underline{v}$ and assuming that the granulate-air mixture is incompressible, mass balance is written as

$$\begin{aligned} &\frac{\partial v_{<1>}}{\partial x^1} + \frac{\partial v_{<2>}}{\partial x^2} + \frac{\partial v_{<3>}}{\partial x^3} \\ + \ &\frac{\partial \zeta}{\partial x^1} x^3 \left(\frac{\partial v_{<2>}}{\partial x^2} + \frac{\partial v_{<3>}}{\partial x^3} \right) + \frac{\partial \zeta}{\partial x^1} v_{<3>} = 0 \quad . \end{aligned} \tag{3}$$

The principle of balance of linear momentum can be written as

$$\vec{\nabla} \cdot \underline{\underline{t}} + \rho\,\underline{b} = \rho\,\underline{a} \quad , \tag{4}$$

where $\underline{\underline{t}}$ is the Cauchy stress tensor, $\underline{b}$ is the body force vector and $\underline{a}$ is the acceleration vector. The equations of motion can be expressed in terms of the physical components as follows:
in the x^1 length direction as

$$\begin{aligned} &\frac{\partial t_{<1\,1>}}{\partial x^1} + 2\frac{\partial \zeta}{\partial x^1} t_{<3\,1>} + \left(1 + \frac{\partial \zeta}{\partial x^1} x^3\right) \left[\frac{\partial t_{<2\,1>}}{\partial x^2} + \frac{\partial t_{<3\,1>}}{\partial x^3} + \rho \mathcal{G} \sin\zeta \right] \\ = \ &\rho \left[v_{<1>} \frac{\partial v_{<1>}}{\partial x^1} + v_{<1>} v_{<3>} \frac{\partial \zeta}{\partial x^1} \right] \\ &+ \rho \left(1 + \frac{\partial \zeta}{\partial x^1} x^3\right) \left[\frac{\partial v_{<1>}}{\partial t} + v_{<2>} \frac{\partial v_{<1>}}{\partial x^2} + v_{<3>} \frac{\partial v_{<1>}}{\partial x^3} \right], \end{aligned} \tag{5}$$

in the x^2 width direction as

$$\begin{aligned} &\frac{\partial t_{<1\,2>}}{\partial x^1} + \frac{\partial \zeta}{\partial x^1} t_{<3\,2>} + \left(1 + \frac{\partial \zeta}{\partial x^1} x^3\right) \left[\frac{\partial t_{<2\,2>}}{\partial x^2} + \frac{\partial t_{<3\,2>}}{\partial x^3} \right] \\ = \ &\rho \left[v_{<1>} \frac{\partial v_{<2>}}{\partial x^1} \right] \\ &+ \rho \left(1 + \frac{\partial \zeta}{\partial x^1} x^3\right) \left[\frac{\partial v_{<2>}}{\partial t} + v_{<2>} \frac{\partial v_{<2>}}{\partial x^2} + v_{<3>} \frac{\partial v_{<2>}}{\partial x^3} \right], \end{aligned} \tag{6}$$

and in the x^3 depth direction as

$$\begin{aligned} &\frac{\partial t_{<1\,3>}}{\partial x^1} + \frac{\partial \zeta}{\partial x^1} (t_{<3\,3>} - t_{<1\,1>}) + \left(1 + \frac{\partial \zeta}{\partial x^1} x^3\right) \left[\frac{\partial t_{<2\,3>}}{\partial x^2} + \frac{\partial t_{<3\,3>}}{\partial x^3} - \rho \mathcal{G} \cos\zeta \right] \\ = \ &\rho \left[v_{<1>} \frac{\partial v_{<3>}}{\partial x^1} - v_{<1>}^2 \frac{\partial \zeta}{\partial x^1} \right] \\ &+ \rho \left(1 + \frac{\partial \zeta}{\partial x^1} x^3\right) \left[\frac{\partial v_{<3>}}{\partial t} + v_{<2>} \frac{\partial v_{<3>}}{\partial x^2} + v_{<3>} \frac{\partial v_{<3>}}{\partial x^3} \right]. \end{aligned} \tag{7}$$

The above forms for the balance of momentum equations are shown in order to emphasize the coupling of many terms with the degree of curvature $\partial\zeta/\partial x^1$ and the depth of the flow x^3.

The boundary conditions need to be defined at the solid surface, or base of the flow, and at the free surface.

By defining the free surface as

$$f = f(x^1, x^2, t) = x^3 \quad , \tag{8}$$

and requiring the local and convected rates of change of f to balance, the well-known kinematic condition is obtained,

$$\frac{\partial f}{\partial t} + \vec{\nabla} f \cdot \underline{v} = 0 \quad , \tag{9}$$

which simply states that the free surface is material, and applies when f is generated by streamlines.

In terms of the physical components, the kinematic condition reads

$$\frac{\partial f}{\partial x^1} v_{<1>} + \left(1 + \frac{\partial \zeta}{\partial x^1} x^3\right) \left[\frac{\partial f}{\partial t} + \frac{\partial f}{\partial x^2} v_{<2>} - v_{<3>}\right] = 0 \quad . \tag{10}$$

A balance of forces at the free surface requires the total traction to vanish there, i.e.

$$\underline{n}\,\underline{\underline{t}} = \underline{0} \quad , at \quad x^3 = f(x^1, x^2, t) \quad . \tag{11}$$

The above condition also applies to a continuous material. Reportedly (see Johnson and Jackson 1987) when this boundary condition is applied to problems concerning granular media, it tends to introduce a singular behavior of the traction in the neighborhood of the interface that is physically unrealistic, as the stress tensor vanishes rapidly through a thickness that is typically less than the thickness of one particle diameter. However, obtaining "depth-averaged" solutions is intended ,and this difficulty should not be a problem, except at the flow boundaries.

Furthermore, it is important to discuss the meaning of a "free surface" in a physical sense. As discussed, it is generally accepted that an avalanche may be considered to be a flow consisting of three distinct regimes. The dense core of the flow is normally obscured by a "dust cloud," which is a layer of highly suspended particulate. From observation, this layer is dominated by the interstitial fluid behavior (Lang et al. 1989). Intuitively, if one defines the "free surface" as the interface of the core of the flow with the turbulent dust cloud, it would be more appropriate to consider the drag at this rough interface rather than a vanishing value of traction. However, it can be demonstrated (McClung and Schaerer 1983) that inclusion of such a term has a negligible effect on the overall resistance to motion of the mass.

With these considerations in mind, the stress-free condition is assumed, and the resulting boundary conditions at the free surface are

$$\begin{aligned}
\frac{\partial f}{\partial x^1} t_{<1\,1>} + \left(1 + \frac{\partial \zeta}{\partial x^1} f\right) \left[\frac{\partial f}{\partial x^2} t_{<2\,1>} - t_{<3\,1>}\right] &= 0 \quad , \\
\frac{\partial f}{\partial x^1} t_{<1\,2>} + \left(1 + \frac{\partial \zeta}{\partial x^1} f\right) \left[\frac{\partial f}{\partial x^2} t_{<2\,2>} - t_{<3\,2>}\right] &= 0 \quad , \\
\frac{\partial f}{\partial x^1} t_{<1\,3>} + \left(1 + \frac{\partial \zeta}{\partial x^1} f\right) \left[\frac{\partial f}{\partial x^2} t_{<2\,3>} - t_{<3\,3>}\right] &= 0 \quad ,
\end{aligned} \tag{12}$$

written in the x^1 , x^2 and x^3 directions respectively.

At the base of the flow, the surface may be described by a function $b = b(x^1, x^2)$, such that the function b may be arbitrarily defined for a given avalanche bed.

The tangency of flow at the base is expressed by the kinematic condition

$$\underline{v} \cdot \underline{n} = 0 \quad , at \quad x^3 = b(x^1, x^2) \quad . \tag{13}$$

Expanding the above in three spatial dimensions yields

$$\frac{\partial b}{\partial x^1} v_{<1>} + \left(1 + \frac{\partial \zeta}{\partial x^1} f\right) \left[\frac{\partial b}{\partial x^2} v_{<2>} - v_{<3>}\right] = 0 \quad , at \quad x^3 = b(x^1, x^2) \quad . \tag{14}$$

Applying the assumption that the basal boundary layer is of a thickness proportional to only a few particle diameters, this layer is neglected. This assumption greatly simplifies the mathematical formulation, as in this layer collisional and frictional stresses must be considered. An appropriate boundary condition has been derived by Hui et al. (1984) for such a case, based on kinetic theory. However, some knowledge of the specularity of particle-wall collisions is required.

By considering only cohesionless, dry granulate, the basal shear traction may be expressed as

$$\underline{n}\,\underline{\underline{t}} - \underline{n}(\underline{n}\,\underline{\underline{t}} \cdot \underline{n}) = -\underline{n}\,\underline{\underline{t}} \cdot \underline{n} \frac{\underline{v}}{|\,\underline{v}\,|} \tan\delta - D_v \,|\, \underline{v} \,|\, \underline{v} \quad , at \quad x^3 = b(x^1, x^2) \quad . \tag{15}$$

where the first term on the right hand side is the Coulomb sliding law, and $\tan\delta$ is the bed friction angle whose value(s) depend on the nature of the particles, degree of packing, and the contact surface. The remaining term on the right-hand side is the boundary drag term. It should be noted that the above is compatible with the kinematic condition at the base (eq 13). When the basal surface agrees with the coordinate generating surface, $\underline{n} = \hat{\underline{e}}_{<3>}$ and the kinematic condition at the base eq 13 reduces to

$$v_{<3>} = 0 \quad . \tag{16}$$

Equation 15 at the base reduces to

$$t_{<3\,1>} = -v_{<1>} \left[\frac{\tan\delta}{|\,\underline{v}\,|} t_{<3\,3>} + D_v \,|\, \underline{v}\,|\right], \tag{17}$$

$$t_{<3\,2>} = -v_{<2>} \left[\frac{\tan\delta}{|\,\underline{v}\,|} t_{<3\,3>} + D_v \,|\, \underline{v}\,|\right] .$$

In view of the experimental work (Lang et al. 1989), which encompassed only the case of the basal surface replicating the coordinate surface, the following discussion will focus on this limiting case. Also, the scaling arguments will demonstrate the inconsequence of weak curvature. For strong curvature in the lateral direction, the theory may be easily reduced to channel flow equations.

Limiting cases of the governing equations

The governing equations that were presented are now nondimensionalized and averaged over the depth and width, in order to provide a set of tractable equations. The nondimensionalization scheme allows for any number of characteristic length scales, that differs from more conventional approaches. Becker (1976) presents a thorough treatment of this method, commonly termed a "distorted model." However he prefers the more distinctive

nomenclature of "Pythagorean method," as the Pythagoreans were motivated by the idea of geometrical proportion being the basis of all things. By applying this method, inspectional analysis indicates limiting forms of the equations that may be more easily treated. The application of this method has been accepted as the appropriate procedure when attempting to model large-scale, geophysical phenomena. By adopting the concept of a "distorted model," consideration of more than one characteristic length scale is allowable. Such an approach is commonly used and applied to large-scale, free-surface flow phenomena such as atmospheric and oceanic motions. A specific example is the well–known "shallow water model." Scaling provides the means to neglect small variations in topography that do not significantly affect the lateral or longitudinal spread of the flowing material. Curvature in the lateral direction will be neglected, as discussed in a later section. For strong curvature in the lateral direction, the equations are easily reduced to a channel flow model.

Also, assumptions are made to simplify the balance equations and boundary conditions. Many of these result directly from the scaling arguments, and others are based on experience with the physical problem at hand The nondimensionalized equations are then averaged over the depth and width of the flow. This is a classical approximation method, commonly applied in evaluating boundary layer flows. The result is a set of equations that represent a balance between the average inertial and resistant forces for each position in the longitudinal direction. Ordering of arguments allows further simplification. The need to consider the detailed character of the flow is thus avoided, and sufficient information for an engineering application is obtained.

Nondimensionalization scheme

At this point, a scheme for nondimensionalization of the governing equations is presented. This step of modeling geophysical phenomena is always to some extent a "leap of faith." That is to say, choosing an appropriate model depends on experience, intuition and explicit dynamic reasoning. The essential dynamic character of the geophysical system must be retained but the validity of the model is examined after the fact.

Although the depth, length and width of an avalanche varies spatially and temporally, it is assumed that characteristic values $\mathcal{L}^i$ may be sensibly chosen such that

$$x^i = \mathcal{L}^i \bar{x}^i \,, \tag{18}$$

where the $\bar{x}^i$ are the nondimensional lengths. The concept of an avalanche as a gravity current suggests the following representation,

$$v_{<i>} = \frac{\mathcal{L}^i}{\mathcal{L}^1} \left[\mathcal{G}\mathcal{L}^1\right]^{1/2} \bar{v}_{<i>} = \mathcal{V}^i \bar{v}_{<i>} \quad . \tag{19}$$

The above may be interpreted with respect to the fluid dynamic concept of "head" or the free fall of a mass point in a gravity field through a given distance, although the length scale may differ. This leads to an expression for time as

$$t = \mathcal{T}\,\bar{t} = \left[\frac{\mathcal{L}^1}{\mathcal{G}}\right]^{1/2} \bar{t} \quad . \tag{20}$$

As the Froude number is the governing parameter for the problem under consideration, the stresses are scaled according to a hydrostatic relationship,

$$t_{<i\,i>} = \rho_o \mathcal{G}\mathcal{L}^3 \cos\zeta_o \, \bar{t}_{<i\,i>} \tag{21}$$

$$t_{<i\,j>} = \rho_o \mathcal{G}\mathcal{L}^3 \sin\zeta_o \, \bar{t}_{<i\,j>} \,, \quad i \neq j \tag{22}$$

where the null subscript denotes a characteristic value for the quantity under consideration, while

$$\sin\tilde{\zeta}_o = \cos\zeta_o \tan\delta \quad . \tag{23}$$

The expression for $\sin\tilde{\zeta}_o$ is a logical choice, as both the driving force and the resistance are represented in eq 23, which both influence the order of magnitude of the resultant shear stresses. The angle ζ may also be characterized as

$$\zeta = \frac{\mathcal{L}^1}{\mathcal{R}}\bar{\zeta} \quad . \tag{24}$$

Also, the following definitions are applied:

$$\epsilon_{ij} = \frac{\mathcal{L}^i}{\mathcal{L}^j} \quad , \tag{25}$$

$$\mathcal{K} = \frac{\mathcal{L}^1}{\mathcal{R}} \quad . \tag{26}$$

In order to evaluate the basal boundary conditions the drag coefficient $\mathcal{D}_v$ is defined in terms of the Voellmy coefficient ϖ , which is traditionally applied to flowing snow, as follows;

$$\mathcal{D}_v = \frac{\rho\mathcal{G}}{\varpi} \quad . \tag{27}$$

ϖ has the units of m/s^2 such that it is a natural choice to scale it with the gravitational constant such that ϖ is related to the dimensionless form $\bar{\varpi}$ by

$$\varpi = \mathcal{G}\bar{\varpi} \quad . \tag{28}$$

Depth and width averaging

When a functional form of solution to a set of governing equations cannot be found, (i.e. a solution that satisfies the equations identically at each point in space and time and that approaches the appropriate boundary values) it may be advantageous to try and satisfy the equations on the average, if the geometry of the problem allows for this approach to result in a meaningful solution. If the equations may be integrated with respect to $\bar{x}^3$ across the depth of flow and with respect to $\bar{x}^2$ across the width of flow, the resulting equations will represent a balance between the average inertial forces and resistant forces for each $\bar{x}^1$ location. In this manner, a velocity distribution may be obtained that satisfies this averaged balance of forces but that does not satisfy the balance at each point across the height and width of the flowing mass.

This method is a classical approximation method that is widely used in examining boundary layer behavior, and was first introduced by von Kármán (1921) and was further improved by Pohlhausen (1921). The results that are obtained from such an approximation are found to be reasonably accurate in many instances. By acknowledging that $\bar{v}_{<1>}$ and $\bar{v}_{<2>}$ are continuous on the interval $[0, \bar{f}]$, the first mean value theorem of calculus ascertains the existence of a point $\wp$ contained in the open interval $(0, \bar{f})$ such that

$$\int_0^{\bar{f}} \bar{v}_{<i>}\, d\bar{x}^3$$

$$= \bar{v}_{<i>}(\wp) \int_0^{\bar{f}} d\bar{x}^3$$

$$= \bar{h}\bar{\bar{v}}_{<i>}\,, \tag{29}$$

and furthermore, it may be assumed that

$$\int_0^{\bar{f}} \bar{v}_{<i>}\, \bar{x}^3\, d\bar{x}^3 \simeq \bar{v}_{<i>}(\wp) \int_0^{\bar{f}} \bar{x}^3\, d\bar{x}^3$$

$$= \frac{\bar{h}^2}{2}\bar{\bar{v}}_{<i>}\,, \tag{30}$$

where the notation $\bar{\bar{v}}_{<i>}$ implies the "depth–averaged" value of $\bar{v}_{<i>}$ and $\bar{f} - 0 = \bar{h}$, the nondimensional flow height. The latter equation is exact if the velocity profile over the depth of the flow is uniform.

Let

$$\epsilon_{3\,1}\epsilon_{3\,2}\,\lambda_{2\,3} = 0(\epsilon_{3\,1}^2) \tag{31}$$

and retain only terms of $0(\epsilon_{3\,1})$. The depth-averaged velocity squared is

$$\overline{\bar{v}^2_{<1>}} = \frac{1}{\bar{h}} \int_o^{\bar{h}} \bar{v}^2{}_{<1>} d\bar{x}^3 \tag{32}$$

where the Boussinesq momentum coefficient will be taken to be near unity such that

$$\overline{\bar{v}^2_{<1>}} \cong \bar{\bar{v}}^2_{<1>}\quad . \tag{33}$$

To be realistic, the Boussinesq coefficient is greater than one, but this approximation is sufficient when the velocity profile is blunt. For a power law velocity distribution (see, for example, Burgers 1924) that typifies a pure Newtonian turbulent fluid, the Boussinesq momentum coefficient is 1.05 (Savage 1989b). The normal stress at the bed is then

$$\bar{t}_{<3\,3>}\Big|_{\bar{x}^3=0} = -\frac{\bar{h}}{\cos\zeta_o}\left[\cos\zeta + \mathcal{K}\frac{\partial\bar{\zeta}}{\partial\bar{x}^1}\bar{\bar{v}}^2_{<1>}\right]. \tag{34}$$

The use of an "earth pressure coefficient" is employed, such that the normal stresses parallel and perpendicular to the path may be equated by employing an earth pressure coefficient $k_{actpass}$

$$\bar{t}_{<1\,1>} = k_{actpass}\bar{t}_{<3\,3>}\quad . \tag{35}$$

$k_{actpass}$ has a value of k_{act} or k_{pass}, determined by the spatial evolution of the pile as either elongation (active case) or contraction (passive case) with respect to the flow direction x^1. From a standard Mohr's circle interpretation, it may be shown that

$$\left.\begin{matrix} k_{act} \\ k_{pass} \end{matrix}\right\} = 2\left[1 \mp \sqrt{1 - (1 + \tan^2\delta)\cos^2\phi}\right]/\cos^2\phi - 1\,, \tag{36}$$

$$\text{for } \partial\bar{\bar{v}}_{<1>}/\partial\bar{x}^1 = \begin{matrix} > 0 \\ < 0 \end{matrix}.$$

It is also assumed that

$$\overline{\bar{v}_{<1>}\bar{v}_{<2>}} = \frac{1}{h}\int_o^{\bar{h}} \bar{v}_{<1>}\bar{v}_{<2>}d\bar{x}^3 \tag{37}$$

and

$$\overline{\bar{v}_{<1>}\bar{v}_{<2>}} \cong \bar{\bar{v}}_{<1>}\bar{\bar{v}}_{<2>}. \tag{38}$$

Also

$$\int_o^{\bar{h}} d\bar{x}^3 \int_{\bar{x}^3}^{\bar{h}} \bar{v}^2{}_{<1>}d\bar{x}^3 \cong \bar{\bar{v}}^2_{<1>}\int_o^{\bar{h}} d\bar{x}^3 \int_{\bar{x}^3}^{\bar{h}} d\bar{x}^3 = \frac{\bar{\bar{v}}^2_{<1>}\,\bar{h}^2}{2}. \tag{39}$$

The integrand $\bar{t}_{<2\,1>}$ is neglected by ordering $\lambda_{2\,1}\,\epsilon_{3\,2} \ll 0(\epsilon_{1\,2})$, as this shear stress would only be locally effective in the case of confined narrow channel flows. It has been shown (Savage 1989 and Lang 1988) that sidewall shearing may be incorporated, if necessary, as an effective friction.

Also

$$\overline{\bar{v}_{<1>}\bar{v}_{<2>}} = \frac{1}{h}\int_o^{\bar{h}} \bar{v}_{<1>}\bar{v}_{<2>}d\bar{x}^3 \tag{40}$$

and assume that

$$\overline{\bar{v}_{<1>}\bar{v}_{<2>}} \cong \bar{\bar{v}}_{<1>}\bar{\bar{v}}_{<2>}. \tag{41}$$

By neglecting the $\bar{t}_{<1\,2>}$ integrand, the lateral pressure gradient may be integrated as

$$\frac{\partial}{\partial\bar{x}^2}\int_o^{\bar{h}} \bar{t}_{<2\,2>}d\bar{x}^3 \cong \frac{\partial}{\partial\bar{x}^2}\left[\frac{k_{\text{actpass}}\bar{h}^2}{2\cos\zeta_o}\left(\cos\zeta + \mathcal{K}\frac{\partial\bar{\zeta}}{\partial\bar{x}^1}\bar{\bar{v}}^2_{<1>}\right)\right] \tag{42}$$

based on the value of the $\bar{t}_{<3\,3>}$ stress component. An approximation for the $\bar{t}_{<3\,2>}$ stress may be made from eq 42 from relating the shear to normal stress such that

$$\int_o^{\bar{h}} \bar{t}_{<3\,2>}d\bar{x}^3 \cong \left\{\frac{\bar{\bar{v}}_{<2>}\bar{h}^2}{2|\,\bar{\bar{\underline{v}}}\,|\lambda_{3\,2}\cos\zeta_o\tan\delta}\left[\left(\cos\zeta + \mathcal{K}\frac{\partial\bar{\zeta}}{\partial\bar{x}^1}\bar{\bar{v}}^2_{<1>}\right)\tan\delta + \frac{|\,\bar{\bar{\underline{v}}}\,|^2}{\bar{h}\,\epsilon_{3\,2}\,\bar{\varpi}}\right]\right\}. \tag{43}$$

The nondimensionalized depth-averaged equations now may be further simplified by width averaging. By defining the (nondimensional) half-width of the pile as

$$b_m = b_m(\bar{x}^1,\,\bar{t}) \tag{44}$$

and assuming that the pile of granulate retains a parabolic shape in the $\bar{x}^1$ plane, the height may be expressed as

$$\bar{h}(\bar{x}^1,\,\bar{x}^2,\,t) \;=\; h_o(\bar{x}^1,\,t)\left(1 - \left(\frac{\bar{x}^2}{b_m(\bar{x}^1,\,\bar{t})}\right)^2\right) \tag{45}$$

where $h_o(\bar{x}^1,\ t)$ is the centerline depth (refer to Figure 1). This assumption is fully supported by the experimental results discussed in Lang et al., 1989. Although natural avalanches do not retain such perfect symmetry due to uneven topography and particle size variations, some degree of symmetry is usually observed in natural avalanche deposition and a parabolic distribution is reasonably replicated.

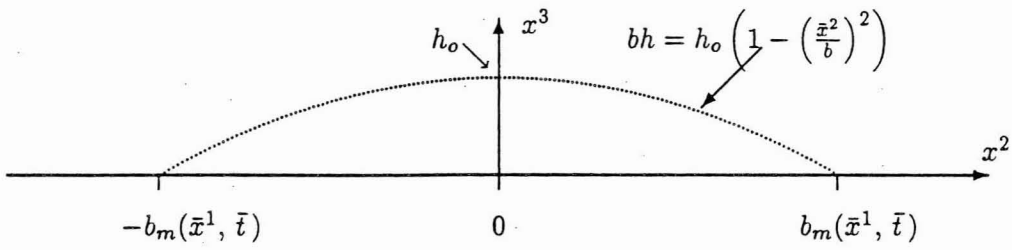

Figure 1: *Approximation of pile shape in the $\bar{x}^1$ plane*

Assuming parabolic symmetry of the pile implies that $\bar{\bar{v}}_{<2>}$, the nondimensional depth averaged lateral pile velocity, varies linearly with respect to $\bar{x}^2$ as in Figure 2 such that

$$\bar{\bar{v}}_{<2>} = \frac{db_m}{dt}\,\frac{\bar{x}^2}{b_m} \quad . \tag{46}$$

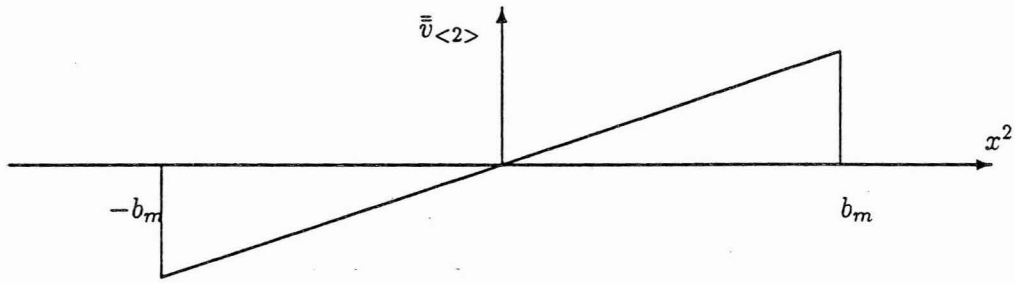

Figure 2: *Lateral pile velocity*

Integrating the continuity eq 3 over the depth and half-width, applying Leibniz' rule, and invoking the symmetry conditions in (45 and 46) gives

$$\frac{\partial}{\partial \bar{x}^1}\int_o^{b_m} \bar{h}\bar{\bar{v}}_{<1>}\,d\bar{x}^2 + \frac{\partial}{\partial \bar{t}}\int_o^{b_m} \bar{h}\,d\bar{x}^2 + \mathcal{K}\in_{3\,1}\frac{\partial \bar{\zeta}}{\partial \bar{x}^1}\frac{\partial}{\partial \bar{t}}\int_o^{b_m}\frac{\bar{h}^2}{2}\,d\bar{x}^2 = 0 \quad . \tag{47}$$

Define a "width"-averaged depth $\tilde{h}$

$$\tilde{h} = \frac{1}{b_m}\int_o^{b_m} \bar{h}\,d\bar{x}^2 \quad . \tag{48}$$

By assuming that the depth has a parabolic distribution in the $\bar{x}^1 = constant$ planes

$$\tilde{h} = \frac{2}{3}\,\bar{h}_o \quad . \tag{49}$$

Furthermore, a depth- and width-averaged velocity may be defined again by use of the mean value theorem of calculus such that

$$\tilde{v}_{<1>} = \frac{1}{b_m \bar{h}} \int_o^b \bar{\bar{v}}_{<1>} \bar{h}\, d\bar{x}^2 \quad . \tag{50}$$

With these, continuity becomes

$$\frac{\partial}{\partial \bar{x}^1}\left(\bar{h}_o\, b_m\, \tilde{v}_{<1>}\right) + \frac{\partial}{\partial \bar{t}}\left(\bar{h}_o\, b_m\right) + \frac{2}{5}\,\mathcal{K}\,\epsilon_{3\,1}\,\frac{\partial \zeta}{\partial \bar{x}^1}\,\frac{\partial}{\partial t}\left(\bar{h}_o^2\, b_m\right) = 0 \quad , \tag{51}$$

Width–averaging of the momentum balance equations requires an approximation for the norm of the velocity vector. By acknowledging that sidewise spreading contributes in a neglible and fairly constant manner to the value of the depth–averaged velocity, one approximation to be considered is

$$|\,\underline{\bar{\bar{v}}}\,| \cong \bar{\bar{v}}_{<1>} \quad . \tag{52}$$

Furthermore, let

$$\begin{aligned}
A &= \epsilon_{3\,2}\, k_{actpass} \quad , \\
B &= \mathcal{K}\frac{\partial \zeta}{\partial \bar{x}^1} \quad , \\
C &= \mathcal{K}\,\epsilon_{3\,1}\,\frac{\partial \zeta}{\partial \bar{x}^1} \quad , \\
F_1 &= \frac{1}{\epsilon_{3\,1}\,\bar{\varpi}} \quad , \\
F_2 &= \frac{1}{\epsilon_{3\,2}\,\bar{\varpi}} \quad , \\
\int_o^b \bar{h}\bar{\bar{v}}_{<1>}\bar{\bar{v}}_{<2>}\, d\bar{x}^2 &\cong \tilde{v}_{<1>} \int_o^b \bar{h}\bar{\bar{v}}_{<2>}\, d\bar{x}^2 \quad ,
\end{aligned} \tag{53}$$

where the last approximation is physically realistic, as the longitudinal velocity has been assumed to have a blunt profile over depth and does not appear to vary over the width at any one transverse section. Applying the aforementioned definitions and approximations to the momentum equation in the $\hat{\underline{e}}_{<2>}$ direction eq 6, and by application of Leibniz' rule, termwise integration from $\bar{x}^3 = 0$ to $\bar{x}^3 = h$ and $\bar{x}^2 = 0$ to $\bar{x}^2 = b_m$ gives

$$\begin{aligned}
&h_o^2\left(\frac{A}{2} + \frac{Ch_o}{3}\right)\left(\cos\zeta + B\tilde{v}_{<1>}^2\right) - \frac{b_m h_o^2}{4\tilde{v}_{<1>}}(\bar{\bar{v}}_{<2>}\Big|_{b_m})\left(1 - \frac{Ch_o}{3}\right)\tan\delta\left(\cos\zeta + B\tilde{v}_{<1>}^2\right) \\
&- \frac{F_2 b_m}{2}\tilde{v}_{<1>}(\bar{\bar{v}}_{<2>}\Big|_{b_m})\left(1 - \frac{Ch_o}{2}\right)
\end{aligned} \tag{54}$$

$$= \frac{\epsilon_{2\,1}}{4}\left\{b_m h_o\left[\tilde{v}_{<1>}\frac{\partial}{\partial \bar{x}^1}(\bar{\bar{v}}_{<2>}\Big|_{b_m}) + \frac{\partial}{\partial \bar{t}}(\bar{\bar{v}}_{<2>}\Big|_{b_m}) + \frac{Ch_o}{3}\frac{\partial}{\partial \bar{t}}(\bar{\bar{v}}_{<2>}\Big|_{b_m})\right] - \frac{C}{15}\frac{\partial}{\partial \bar{t}}(b_m h_o^2)\right\}.$$

The above equation is easily obtained by simple integration by noting that

$$\bar{h}\Big|_{b_m} = 0$$

$$\bar{\tilde{v}}_{<2>}\Big|_{o} = 0 \quad .$$

Similarly, let

$$G = \epsilon_{3\,1}\, k_{actpass} \quad . \tag{55}$$

By the same method the width–averaged momentum balance in the $\hat{\underline{\varepsilon}}_{<1>}$ direction is

$$\begin{aligned} & -\frac{3G}{4b_m h_o}\frac{\partial}{\partial \bar{x}^1}\left[\frac{2b_m h_o^2 \cos\zeta}{3} + \frac{8b_m h_o^2 B \tilde{v}_{<1>}^2}{15}\right] - \left(1 - \frac{4h_o C}{5}\right)\left[\cos\zeta\tan\delta + B\tilde{v}_{<1>}^2\tan\delta\right] \\ & - F_1\tilde{v}_{<1>}^2\left(\frac{3}{2b_m h_o} - C\right) + \left(1 + \frac{2h_o C}{5}\right)\sin\zeta \\ = \; & \frac{\partial \tilde{v}_{<1>}}{\partial \bar{t}} + \tilde{v}_{<1>}\frac{\partial \tilde{v}_{<1>}}{\partial \bar{x}^1} + \frac{2Ch_o}{5}\frac{\partial \tilde{v}_{<1>}}{\partial \bar{t}} \\ = \; & \frac{d\,\tilde{v}_{<1>}}{d\,\bar{t}} \end{aligned} \tag{56}$$

Equations 51, 56, and 54 comprise a complete boundary value problem for the free surface flow of a cohesionless granulate down an open terrain of variable curvature in the longitudinal direction. The requirement of pile symmetry has been imposed, which is satisfied by the experiments in Lang et al. (1989), that meet the criteria of being friction–governed flows.

NUMERICAL SOLUTIONS AND COMPARISON TO EXPERIMENTS

Because a closed form solution is not available for the system of equations which was outlined, a numerical solution must be sought. Savage and Hutter (1989) show that a Lagrangian formulation is the natural choice for this system of equations in order to determine the position of the granulate surface through time. With this method, the boundaries of the finite difference grid are convected with the depth- and width-averaged velocities of the granular material.

Two different models are developed. First, the boundary drag term is neglected and predictions are based solely on modelling the material with the Coulomb friction law. Then, it is demonstrated that a flow transition regime exists where the boundary drag term must be included in the model in order to predict the position of the pile through time, and more specifically, the final runout zone position. An artificial viscosity term $\mu\partial^2 u/\partial x^2$ is added to the equation of motion in order to smooth the solution.

Unconstrained Coulomb flow model with constant bed friction

Now the depth- and width-averaged balance equations are solved. In addition to predicting the length, height and longitudinal velocity through time, the sidewise spreading and rate of sidewise spreading may be determined. The results from channel flow models (Lang 1988) are used as a guideline. A first approximation is applied, where it is assumed that

the boundary drag term may be neglected, and that δ remains constant through the length of the pile. This provides the simplest set of width-averaged equations. For this system of equations, the condition is applied that $C << 1$. The depth- and width-averaged equations as presented are then simplified. For comparison with simple laboratory findings a constant bed friction angle provides good results. This model was tested against the experimental results presented in Lang et al 1989. The numerical model and laboratory results show reasonable agreement. For example, experiment DA029 was released at an initiation zone angle of 35^o. DA029 consisted of 20.0 kg of 2- to 3- mm quartz particles, reaching a maximum velocity of 3.6 m/s at 0.9 s. Figure 3 shows the experimental values of velocity and position for the leading and trailing edges through time as compared with the theoretical predictions. The leading edge is the point on the $\bar{x}^2 = 0$ axis that travels the farthest, and the trailing edge is the point on the $\bar{x}^2 = 0$ axis that travels the least amount of distance through time. Due to the method of photography (see Lang et al 1989), a nondimensional time error of 0.52 may be incurred in determining the initial frame, which may result in some of the offset. Nevertheless, the theory predicts the general characteristics of the longitudinal progress of the granular mass, and the final position of the forward edge in the runout zone is accurately predicted. The prediction of the position and velocity of the leading edge of an avalanche is the critical information required to calculate the impact pressure on a structure and to motivate zoning restrictions.

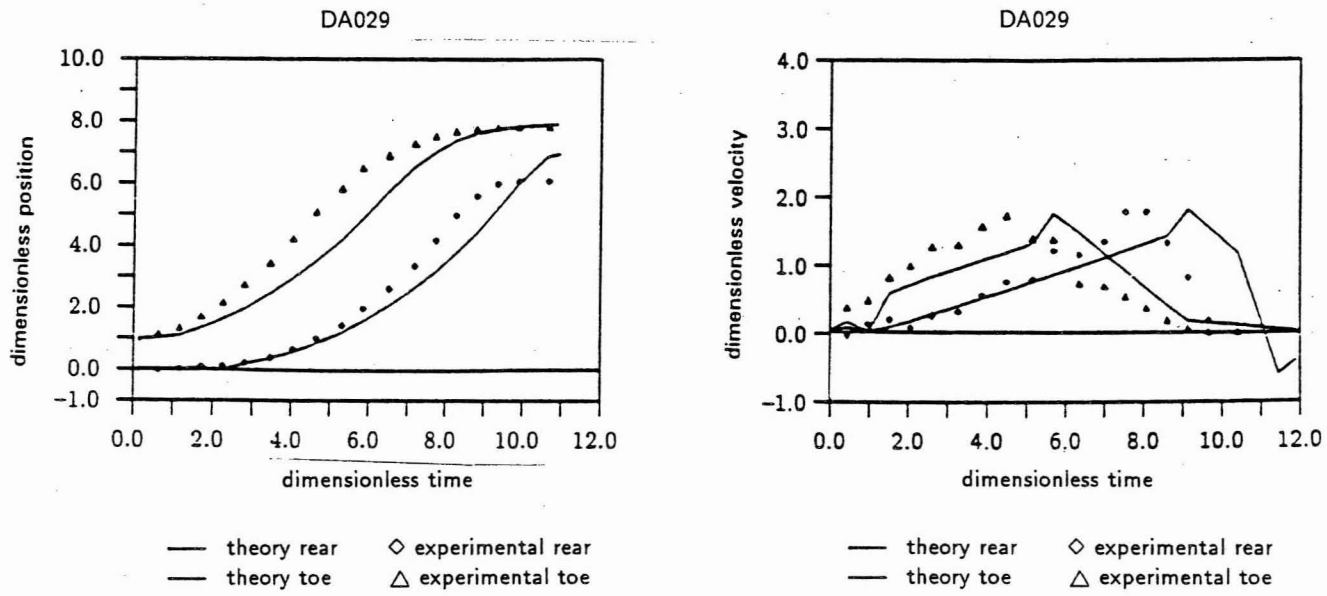

Figure 3: *Theoretical predictions and experimental values of nondimensional position and velocity of the leading and trailing edge as a function of nondimensional time for experiment DA029*

In Figure 4 the progression of the width and height at selected time increments is presented. The time increments were chosen to correspond with frame times. The left hand side of the figure represents the progression of the half width of the model and experiment (see Lang et al 1989) at selected time increments, and the right hand side is the predicted depth profile through time. Due to limited space in the laboratory, it was not possible to record the height of the pile through time, but the general features are reasonably reproduced by the theory; that is, the pile collapses rapidly, elongates and flattens to a maximum prior to

encountering the runout zone. Then as the forward portion of the pile stops, the trailing edge retains momentum and piles up over the static portion. When the angle of repose is exceeded, the pile relaxes back to the internal angle of friction, and the tail comes to rest at some angle less than the angle of repose (Fig. 4). The maximum final (nondimensional) pile height was measured to be 0.21, and the model predicts 0.23. The model overestimates the (dimensional) lateral spread of the pile, by approximately 9%, and the overestimation of the lateral spread causes the underestimation of the pile length through time, particularly in the runout zone. The pile is predicted to spread more rapidly in the lateral direction in the initiation zone.

For experiments that were conducted at an initial bed angle (or starting zone angle) of 35^o, the constant bed friction angle model is a good predictor. For laboratory simulations conducted with greater starting zone angles, the model greatly overpredicts the final position of the granulate mass in the runout zone. For example, experiments DA025 and DA033 were also modeled with the constant bed friction model. Both of these experiments were released at an initiation angle of 45^o. For DA025, 20.0 kg of 2- to 3- mm quartz particles were used. The resulting predictions of position and velocity through time show that the final positions of the leading edge and the tail are greatly overpredicted. Position and velocity profiles for DA033 18.4 kg of 2-3 mm *marmor* show also that the toe and tail positions are overpredicted with this model (for details, see Lang 1992).

This result agrees with problems encountered when attempting to model natural snow avalanches. Gubler (1987) discusses the problem of modeling higher speed avalanches with traditional avalanche models. The friction coefficients must be increased by a factor of 2, in general, in order to force the avalanche to come to rest in the appropriate position in the runout zone.

Because this numerical model accurately predicts the experiments conducted at 35^o which results in lower velocities and accelerations than for larger angles, it is possible that a transition in flow regime occurs in the boundary layer where the boundary drag force becomes non-negligible at higher velocities. Its inclusion in the numerical model is presented in the following section. Gubler (1987) discusses a similar flow regime transition for natural snow avalanches from *flexible sliding body* to *partial fluidization*. Furthermore, Buser and Frutiger (1980) found that the inclusion of both sliding bed friction and boundary drag underpredict velocities for very large natural snow avalanches. This result may also be an indication of flow transition behavior, in the sense that an avalanche may initiate in the *flexible sliding body* type flow and reach a transitive velocity where *partial fluidization* occurs. If the additional resistance due to boundary drag is applied throughout the flow time, the theory would underpredict velocities. However, if a critical velocity could be determined that would predict the transition, and hence the appropriate application of an additional boundary drag term, perhaps this problem could be circumvented.

Unconstrained Coulomb flow with boundary drag term

It was mentioned in the previous discussion that the constant bed friction angle model becomes a poor predictor for initiation zone angles greater that 35^o. At this point it seems sensible to attempt to model the additional resistance to flow by inclusion of the boundary drag term. Again, average values are used to avoid the possibility of the pile height approaching zero. Also, the depth- and width-averaged drag term includes the width of the pile in the denominator, that is zero at the midpile. Therefore, the following average of the drag term is included:

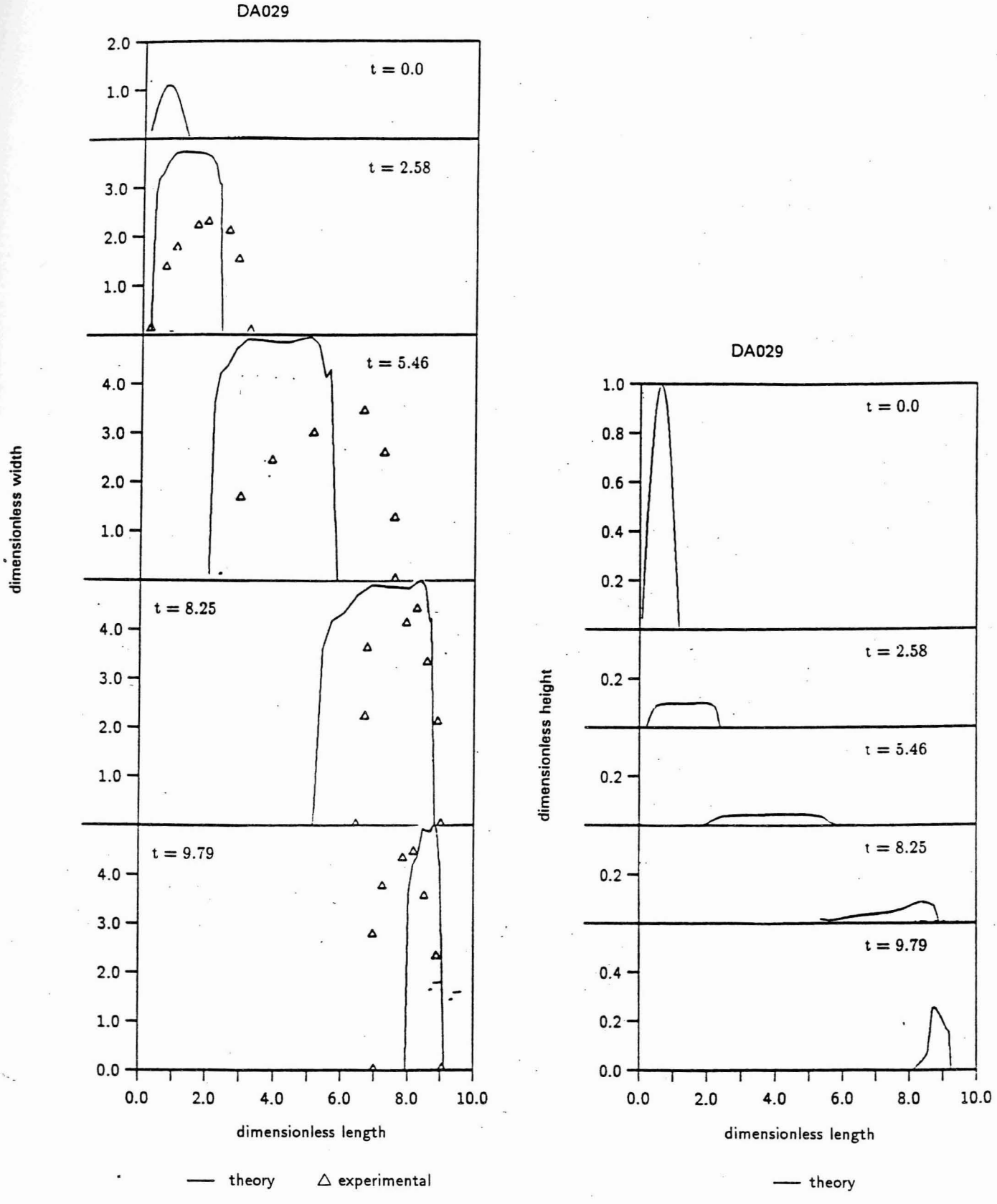

Figure 4: *Sequence of nondimensional computed and experimental pile width and computed pile height at frame time increments for DA029*

$$-\frac{3\,\mathcal{G}\,u_{av}^2}{2\,\epsilon_{3\,1}\,\bar{\varpi}\,h_{av}\,b_{av}} \tag{57}$$

As an example, experiment DA025 was modeled with the inclusion of the drag term, and results are presented in Figures 5 and 6. DA025 was conducted at an initiation angle of 45° and 20.0 kg of 2-3 mm quartz particles were used. Figure 5 depicts the resulting predictions of position and velocity through time. The final position of the leading edge is somewhat underpredicted, but the general motion of the pile through time is well mirrored. The model does not allow the maximum leading edge velocity to be attained. It may be restated that ideally, the boundary drag term should perhaps be applied only when a critical velocity (or critical Froude number) is attained.

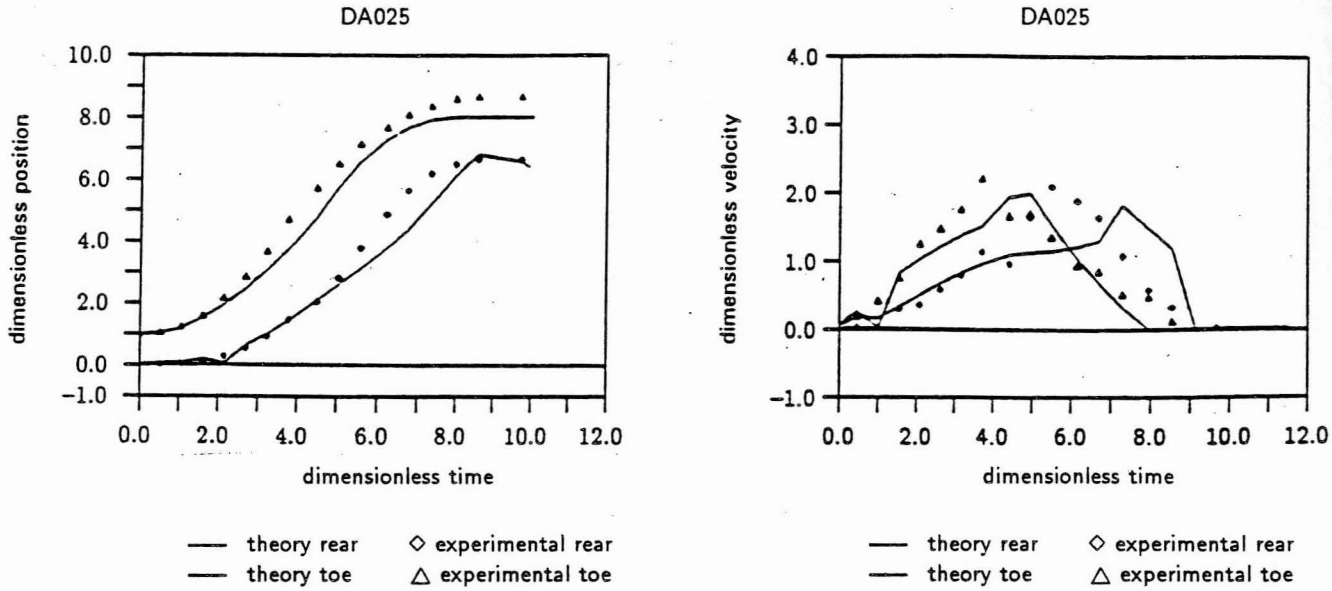

Figure 5: *Theoretical predictions and experimental values of nondimensional position and velocity of the leading and trailing edge as a function of nondimensional time for experiment DA025*

As shown in Figure 5, the initial spread of the pile is overpredicted, but in the runout zone, the shape is quite accurately replicated. The pile is predicted to be shorter in the longitudinal direction and slightly wider than the actual pile shape. The final maximum (nondimensional) pile height is extremely accurate: the theory predicted 0.205 and the experimental result was 0.206.

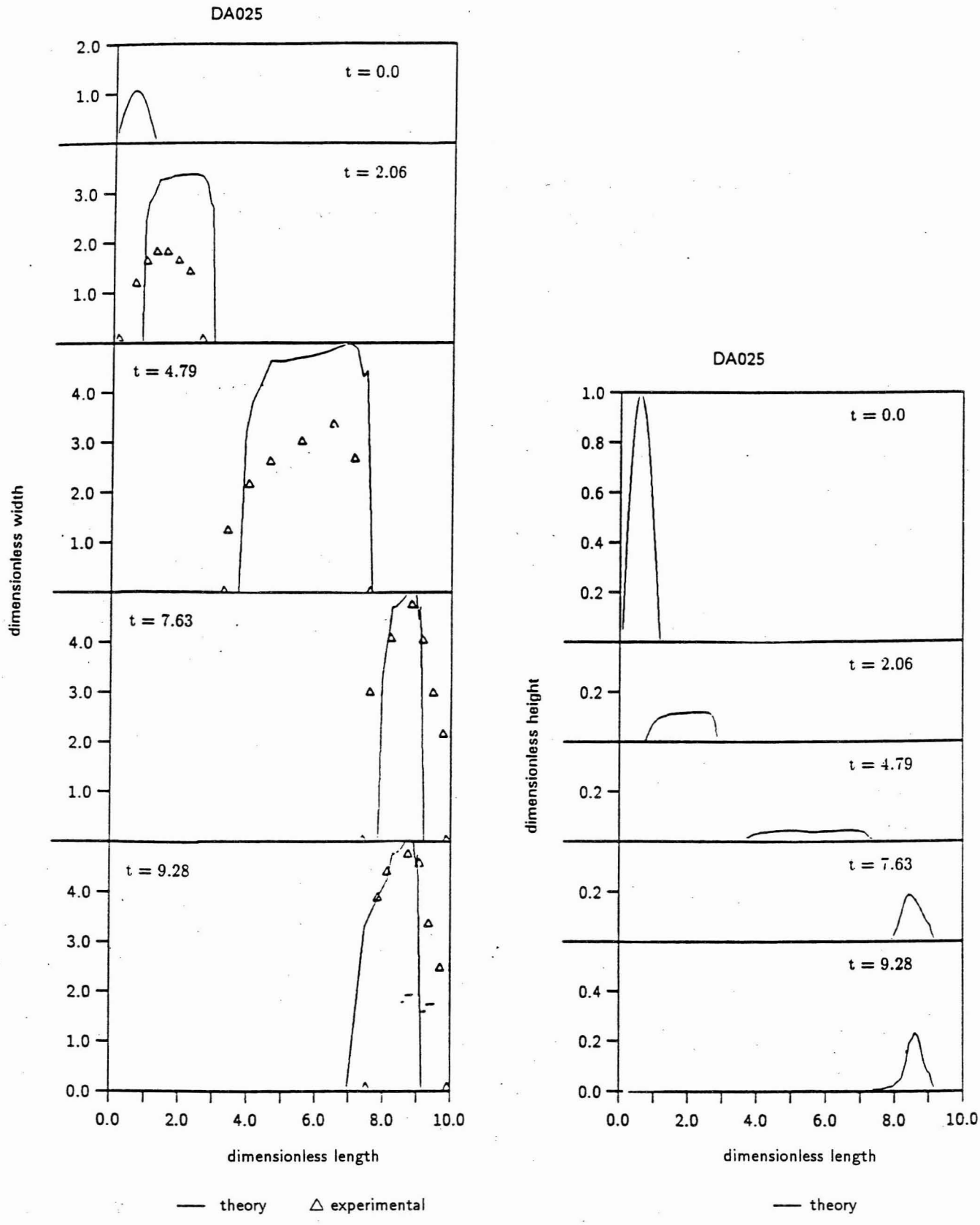

Figure 6: *Sequence of nondimensional computed and experimental pile width and computed pile height at frame time increments for DA025*

CONCLUSIONS AND REMARKS

Governing equations and closure relations were proposed to represent the flow of a cohesionless granular medium on any given topography. The goal was to develop an easily applied model to predict the bulk flow characteristics of the mass of granulate. Indeed, the anticipated result of every avalanche model is to predict the final runout zone position of the mass and the possible impact pressures on structures in the path of an avalanche. A purely mechanical theory was proposed and the granular mass was treated as a continuum. The balance equations in terms of physical components in an adaptable and appropriate coordinate system were derived. A constitutive assumption was justified by considering the different flow regimes in question, and the experimental results from Lang et al. (1989), and other investigations.

The governing equations were nondimensionalized and averaged over the depth and width, in order to provide a set of tractable equations. The nondimensionalization scheme allows for any number of characteristic length scales, which differs from more conventional approaches. By applying this method, inspectional analysis indicates limiting forms of the equations that may be more easily treated. The application of this method has been accepted as the appropriate procedure when attempting to model large scale, geophysical phenomena. Assumptions were made to simplify the balance equations and boundary conditions, which resulted directly from the scaling arguments or were based on experience with the physical problem at hand. Changes in the volume fraction of the granulate and variations in topography in the lateral direction were neglected. The nondimensionalized equations were then averaged over the depth and width of the flow, a classical approximation method, commonly applied in evaluating boundary layer flows resulting in a set of equations which represent a balance between the average inertial and resistant forces for each position in the longitudinal direction. With this method, no information can be provided to determine the detailed character of the flow, but sufficient information for an engineering application is obtained.

A Lagrangian discretization scheme was applied in order to numerically evaluate the magnitude of velocity, and predict the spatial evolution of the granular pile through time. This type of analysis allows for the particulate to be advected with the finite difference grid, and was shown by Savage and Hutter (1989) to be the appropriate choice for such a problem.

Two models were developed for the free surface flows. The first assumed a constant bed friction angle, and neglected any boundary drag effects. This model proved to be adequate in predicting the experiments discussed in Lang et al. (1989), which were conducted at bed surface angles of 35^o, but failed for larger values of initiation zone angles. The method of photography incurred a nondimensional time error of 0.52 in determining the initial frame, which may have resulted in some of the inaccuracy. Nevertheless, the theory accurately predicts the general characteristics of the longitudinal progress of the granular mass, the velocity with time, and the final position of the forward edge in the runout zone for the 35^o experiments (e.g., DA029). The progression of the height and width at selected time increments, corresponding with frame times, was also well reproduced by the theory. The pile collapses rapidly, elongates and flattens to a maximum prior to encountering the runout zone. Then as the forward portion of the pile stops, the trailing edge retains momentum and piles up and over the static portion. When the angle of repose is exceeded (Fig. 4) the tail reverts back to an angle equivalent to or less than the internal angle of friction. The final angle (actual or predicted) depends on the amount of backwashing that occurs. The maximum final (nondimensional) pile height was predicted to within 8%. The model overestimates the lateral spread of the pile and this causes the underestimation of the pile length through time, particularly in the runout zone. The pile is predicted to spread more rapidly in the initiation zone. But the average flow procession of the pile is well predicted.

For laboratory simulations conducted with greater starting zone angles, the model that

neglects any flow resistance due to drag overpredicts the final position of the granulate mass in the runout zone. This result agrees with problems encountered when attempting to model natural snow avalanches. Attempting to model higher speed avalanches with a basic, or all-encompassing, avalanche model, and producing erroneous results is not a new or surprising problem. Gubler (1987) discusses the problem of increasing friction coefficients by a factor of 2, in general, in order to force avalanche models to come to rest in the appropriate position in the run-out zone, when attempting to model snow avalanches that attain higher velocities.

Since the first model breaks down for initiation zone angles greater that 35^o, an attempt was made to model the additional resistance to flow by inclusion of the boundary drag term. Experiment DA025 was modeled with the inclusion of the boundary drag term, and results were presented in Figures 5 and 6. This experiment was released at an initiation angle of 45^o.

For DA025, the final position of the leading edge was underpredicted, but the general motion of the pile through time is well mirrored. The model does not allow the maximum leading edge velocity to be attained. It is not an unreasonable idea that the boundary drag term should perhaps be applied only when a critical velocity (or critical Froude number) is attained. Also, the initial spread of the pile was overpredicted, but in the runout zone, the shape is quite accurately replicated. The pile is predicted to be shorter in the longitudinal direction and slightly wider than the actual pile shape. The final maximum (nondimensional) pile height was accurately predicted, with a theoretical value of 0.205 compared to the experimental result of 0.206.

In general, the numerical models and experiments show good agreement and provide valuable information. These results are justification for the characterization of the flow, and persuance of averaged quantities. The resulting predictions of geometry and velocity through time are encouraging. However, some subjectivity is still required to determine appropriate constitutive parameters and it is unknown if the models can represent naturally occurring events.

Future work should include testing these models against naturally occurring events, in particular, snow avalanches, since experimental data are available (Gubler, 1987). This would be no minor task, considering one would have to attempt to determine in-situ properties of the snowpack. Also, the model presented was developed to include curvature variations of the slide path in the lateral direction. If one were to completely test the model against a naturally occurring event, it would have to be determined how important the topographical variations in the lateral direction are in affecting the final runout position. Certainly, constraining the flow in a channel prohibits dilatation to some degree. This would entail more experimental work on simple materials. It may be sufficient to characterize a given natural topography by simply combining the channel flow and unconstrained flow models, and specifying the channel width as a function of longitudinal direction, and the position(s) where channel flow is no longer appropriate. Asymmetry in the spreading direction may or may not be a decisive factor in determining the final runout position of the flow.

Also, in order to compare the model to snow avalanches one must remain cognizant of the fact that the cohesive nature of snow has been neglected. This omission is probably most impractical for modeling the initiation of the avalanche and the final stages of compaction in the runout zone, but it is unknown if neglecting cohesion plays a significant role in determining the salient features of the flow. The same statement may be made concerning particle size distribution. It is sufficient to say that some progress has been made in modeling granular flows, but efforts should continue to resolve these and many other issues.

LITERATURE CITED

Becker, H.A. (1976) Dimensionless parameters: Theory and methodology. *Applied Science Publishers, Ltd., London* 128 pp. 24-29.

Brown, R.L. (1976) A thermodynamic study of materials representable by integral expansions. *International Journal of Engineering Science*, **14**(11) 1033-1046.

Brown, R.L. (1976) A fracture criterion for snow. *Journal of Glaciology*, **19**(81) 111-121.

Brown, R.L. (1979) A volumetric constitutive law for snow subjected to large strains and strain rates. *U.S. Army Cold Regions Research and Engineering Laboratory Report 79-20*

Brown, R.L. (1980a) Pressure waves in snow. *Journal of Glaciology*, **25**(91) 99-107.

Brown, R.L. (1980b) An analysis of non-steady plastic shock waves in snow. *Journal of Glaciology*, **25**(92) 279-287.

Brown, R.L. and T.E. Lang (1973) On the mechanical properties of snow and it's relation to the snow avalanche. *Proceedings, Annual Engineering Geology Soils Engineering Symposium* 11^{th}. 19-36.

Brown, R.L., T.E. Lang, W.F. St. Lawrence and C.C.Bradley (1973) A failure criterion for snow. *Journal of Geophysical Research*, **78**(23). 4950-4958.

Brugnot, G. (1979) Recent progress and new applications of the dynamics of avalanches. *Proceedings Snow in Motion Symposium, International Glaciological Society*

Buser, O. and H. Frutiger (1980) Observed maximum runout distance of snow avalanches and the determination of the friction coefficients μ and ξ. *Journal of Glaciology*, **26**(94) 121-130.

Dent, J.D. and T.E. Lang (1980) Modelling of snow flow. *Journal of Glaciology*, **26**(94). 131-140.

Dent, J.D. and T.E. Lang (1981) Experiments on the mechanics of flowing snow. *Cold Regions Science and Technology*

Gubler, H.-U. (1987) Measurements and modelling of snow avalanche speeds. In *Avalanche Formation, Movement and Effects, International Association for the Hydrological Sciences Publ. No. 162* (ed. B. Salm and H.-U. Gubler), 405-420.

Hansen, A.C. (1985) A constitutive theory for high rate multiaxial deformation of snow. Ph.D. Dissertation, Montana State University

Hansen, A.C. and R.L. Brown (1986) The granular structure of snow: an internal state variable approach. *Journal of Glaciology*,**32**(112). 434-439.

Hui, K., P.K. Haff, J.E. Ungar and R. Jackson (1984) Boundary conditions for high shear grain flows. *Journal of Fluid Mechanics* **145** 223-233.

Hutter, K., Ch. Plüss and N. Maeno (1988) Some implications deduced from laboratory experiments on granular avalanches. No. 94 der Versuchsanstalt für Wasserbau, Hydrologie und Glaziologie an der ETH, 323-344.

Lang, R.M. (1988) A numerical study on channel flows of cohesionless granular media with variable basal friction and Voellmy type drag. *Eidgenossiche Institut fuer Schnee und Lawinen Forschung Report.*

Lang, R.M., B.R. Leo and K. Hutter (1989) Flow characteristics of an unconstrained non-cohesive granular medium down an inclined, curved surface: Preliminary experimental results. *Annals of Glaciology* **13** 146-153.

Lang, R.M. (1992) An experimental and analytical study on gravity driven free surface flows of cohesionless granular media. Doctoral Dissertation, Technische Hochschule Darmstadt.

Lang, T.E. and J.D. Dent (1980) Scale modelling of snow avalanche impact on structures. *Journal of Glaciology* **26***(94)* 189-196.

Lang, T.E. and J.D. Dent (1982) Review of surface friction, surface resistance, and flow of snow. *Reviews of Geophysics and Space Physics* **20***(1)*. 21-37.

McClung, D. and P.A. Schaerer (1983) Determination of avalanche dynamics friction coefficients from measured speeds. *Journal of Glaciology*, **26**(94) 109-120.

Mellor, M. (1968) Avalanches. U.S. Army Cold Regions Research and Engineering Laboratory Monograph III A3d.

Nakamura, H. et al. (1987) A newly designed chute for snow avalanche experiments. In *Avalanche Formation, Movement and Effects, International Association for the Hydrological Sciences Publ. No. 162* (ed. B. Salm and H.-U. Gubler), 441-451.

Norem, H., T. Kvisterøy and B.D. Evensen (1985) Measurement of avalanche speeds and forces: instrumentation and preliminary results of the Ryggfonn project. *Annals of Glaciology*, **6** , 19-22.

Pao, R.H.F. (1961) Fluid Mechanics. New York: John Wiley.

Perla, I.P., T.T. Cheng and D.M. McClung (1980) A two-parameter model of snow avalanche motion. *Journal of Glaciology*, **26** (94), 197-207.

Plüss, Ch. (1987) Experiments on granular avalanches. Diplomarbeit, Abteilung X, Eidgenossische Technische Hochschule, Zürich, 113 pp.

Pohlhausen,K. (1921) Zur näherungsweisen Integration der Differentialgleichung der laminaren Grenzschicht. *Zeitung fuer Angewandte Mechanik und Mathematik* 1 252-268.

Salm, B. (1966) Contribution to avalanche dynamics. *International Association for the Hydrological Sciences AISH Publ., 69.* 199-214.

Salm, B. (1971) On the rheological behaviour of snow under high stresses. *Contrib. Inst. Low Temp. Sci. Hokkaido Univ., Ser. A, 23.* 1-43.

Salm, B. (1975) A constitutive equation for creeping snow. *International Association for the Hydrological Sciences AISH Publ., 114.* 222-235.

Salm, B. (1977) Eine Stoffgleichung für die kriechende Verformung von Schnee. Dissertation 5861, Eidgenossische Technische Hochschule Zürich

Savage, S. B. (1983) Granular flows down rough inclines: Review and extension. *Mechanics of Granular Materials: New Models and Constitutive Relations* (ed J.T. Jenkins and M. Satake). Amsterdam: Elsevier, 261-82.

Savage, S. B. (1984) The mechanics of rapid granular flows. *Advances in Applied Mechanics* **24** (ed T.Y Wu and J. Hutchinson). New York: Academic, 289-366.

Savage, S. B. and K. Hutter (1989) The motion of a finite mass of granular material down a rough incline. *J. Fluid Mech.* **199**, 177-215.

Savage, S. B. (1989) Flow of granular materials. *Theoretical and Applied Mechanics, Elsevier Sci. Pub., IUTAM.* 241-266.

Siemes, W. and L. Hellmer (1962) *Chem. Eng. Sci.*, **17**, 555.

St. Lawrence, W.F. (1977) A structural theory for the deformation of snow. Ph.D. Dissertation, Montana State University

St. Lawrence, W.F. and T.E. Lang (1981) A constitutive relation for the deformation of snow. *Cold Regions Science and Technology*, 4 3-14.

Szidarovszky, F., K. Hutter and S. Yakowitz (1987) A numerical study of steady plane granular chute flows using the Jenkins-Savage model and its extension. *International Journal for Numerical Methods in Engineering*, **24** 1993-2015

Voellmy, A. (1955) Über die Zerstörungskraft von Lawinen. *Schweizerische Bauzeitung* **73**, 159-162, 212-217, 246-249, 280-285

von Kármán, Th. (1921) Über laminare und turbulente Reibung. *Zeitung fuer Angewandte Mechanik und Mathematik* 1, 233-252.

ACKNOWLEDGMENTS

This work was completed at the Technische Hochschule Darmstadt, Federal Republic of Germany. Dr. Stuart B. Savage provided guidance in the completion of this work. The authors thank Heinz Wall and all the employees in the laboratory and machine shop at the Technische Hochschule Darmstadt, whose cooperation was exemplary.

NOMENCLATURE

z^i	Cartesian coordinates
x^i	curvilinear coordinates
$\underline{g}_i$	natural basis for curvilinear system
g_{ij}	metric of the space
$\underline{\hat{e}}_{<i>}$	orthonormal basis for curvilinear system
$\underline{v}$	underline denotes first order tensor (vector)
$\underline{\underline{t}}$	double underline denotes second order tensor
ζ	angle defining longitudinal variations from the horizontal
$v_{<i>}$	physical component of $\underline{v}$
ρ	mass density
$\vec{\underline{\nabla}}$	del operator, operating on the argument indicated by arrow
$t_{<ij>}$	physical component of $\underline{\underline{t}}$, for the stress tensor with the subscripts implying on the i surface and in the j direction
f	function defining free surface
b	function defining bed surface
$\underline{n}$	unit normal vector
$\underline{v}$	velocity vector
$\underline{b}$	body force vector
$\underline{a}$	acceleration vector
$\underline{\underline{t}}$	Cauchy stress tensor
δ	bed friction angle
ϕ	internal friction angle
$\mathcal{D}_v$	boundary drag coefficient
$\mathcal{L}^i$	i^{th} characteristic length scale
$\mathcal{G}$	acceleration due to gravity
$\mathcal{T}$	characteristic time scale
$\bar{x}$	overbar denotes nondimensional quantity
$\bar{\bar{x}}$	double overbar denotes nondimensional, depth-averaged quantity
$\tilde{x}$	tilde denotes nondimensional, depth- and width-averaged quantity
$\in_{ij}$	ratio of $\mathcal{L}^i$ (i^{th} characteristic length scale) to $\mathcal{L}^j$ (j^{th} characteristic length scale)
ϖ	Voellmy coefficient